# DRAFT        OMAE2016-54277

# THE INFLUENCE OF EXTERNAL BOUNDARY CONDITIONS ON ICE LOADS IN ICE-STRUCTURE INTERACTIONS

**Regina Sopper, Claude Daley,**
**Bruce Colbourne, Stephen Bruneau**
Memorial University of Newfoundland
St. John's, Newfoundland and Labrador,
Canada

## ABSTRACT

*Design ice loads are generally derived from field measurements or laboratory experiments. The latter commonly neglect the circumstance that most ice-structure interactions occur underwater, despite the fact that studies report higher ice loads if water is present. Other than a few studies on ice extrusion processes, most investigations on ice loads also do not specifically consider the presence of snow or granular ice at the ice-structure interface. To elucidate the influence of water, snow and crushed ice, as external boundary conditions, on ice load magnitude, 71 small-scale laboratory tests were carried out. Testing involved a hydraulic material testing system (MTS machine) located in a cold room at -7°C. Ice specimens were conical shaped with 25 cm in diameter and with 20° and 30° cone angles. Those were impacted with a flat indentation plate at 1 mm/s, 10mm/s and 100 mm/s indentation rates. Time-penetration and time-force histories from the MTS machine, as well as qualitative contact area and local pressure measurements from tactile pressure sensors were collected. Tests were also recorded with a high speed camera and monitored with still photos. The effect of submergence was most evident at high indentation rate, yielding high ice loads. Snow and granular ice caused comparably high ice loads at the high indentation rate. Moreover, the snow and granular ice conditions also dramatically increased loads at the low indentation rate. In all cases, higher ice loads were associated with increased effective contact areas.*

## INTRODUCTION

Icebergs still pose a significant risk of damage to marine structures. In 2000, Hill [1] introduced an iceberg collision database with information on environmental conditions, and damage severity. The database comprises 670 events between 1810 and 2004 involving fishing boats, passenger ships, tankers, bulk carriers and freighters. In just above one quarter of the events, the vessel sank or had to be abandoned. The numbers of accidents and extent of damage reveal the need for measures to reduce risks and damage.

Field studies that naturally involve ice impacts in water are most often conducted with instrumented ships. For instance, Masterson and Frederking [2] examined local pressures and forces on icebreakers that rammed ice floes. Later, in 2001, the Canadian Coast Guard Ship Terry Fox was equipped with strain gauges and 178 ice impacts with bergy bits (up to 20,000 t) were accomplished (Ritch et al. [3]). However, those studies do not allow a comparison with loads derived under dry circumstances to directly assess the effect of the water. Most other field indentation tests focus on the influence of different indenter shapes (e.g. Frederking et al. [4], Masterson et al. [5], Kennedy et al. [6]) but not on external boundary conditions.

This is despite the fact that ice-structure interactions most likely occur underwater, or at least partially underwater. Ice strength information is often derived from laboratory dry tests and laboratory experiments are still essential to investigate the processes involved in ice-structure interactions. There are only a few publications that address the influence of submergence during an ice impact. For example a layer of spray water was found to yield higher ice loads compared to a dry impact (Varsta [7]).

A first approach was taken in a recent laboratory study (Sopper et al. [8]) on ice impacts that provides clear evidence that submergence significantly influences ice loads, particularly at high indentation rates. Furthermore, little information exists on the difference that snow or granular ice at the ice-structure interface cause in ice load magnitude, and how this compares to other external boundary conditions. Most studies focus on ice

extrusion processes (Tuhkuri and Riska [9], Spencer et al. [10]), the characterization of the material properties (Singh and Jordaan [11]), or the effect on the local pressure distribution (Daley et al. [12]).

This paper presents some results of a study that takes a first step to quantify the importance of different external boundary conditions in ice load magnitude and to elucidate the reasons for the observed phenomena.

## EXPERIMENTAL SETUP

The tests took place in a refrigerated chamber (cold room) at an ambient temperature of -7°C. Testing apparatus was a 500 kN closed-loop controlled compressive loading machine (MTS machine) operated via displacement control. All tests were performed inside a watertight aluminum container (Figure 1) that enabled the testing in different environmental conditions. The inside dimensions of the container were 40 cm x 40 cm by a height of 37 cm, leaving a clear distance of 7 cm on either side of the ice specimen. The indenter was a flat aluminum plate with a cross-sectional base area of 35 cm x 35 cm on the bottom of the container. Visual observations and high speed camera (HSC) recordings were facilitated by 24.8 cm x 31.1 cm acrylic windows on each side of the container. The container was attached to the actuator of the MTS machine that moved upwards towards the fixed crosshead with the load cell. A 5 cm diameter bolt screwed into that load cell, holding a steel plate with the ice specimens mounted to it.

### Ice Holder

The specimens were grown in ice holders consisting of 25 cm in diameter and 5 cm tall steel rings. Flanges were welded around the rings building the bottom of the ice holders and facilitated the attachment to the MTS machine with four bolts.
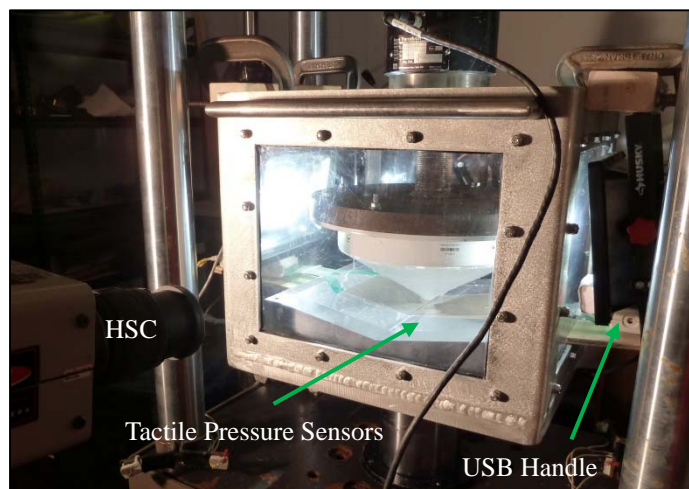


**Figure 1:** Experimental set-up.

### Ice Specimen

The ice specimens were 20° and 30° ice cones with ice strength similar to that of multi-year ice. They were laboratory fabricated according to the procedure developed by Bruneau et al. [13] and as in detail described in Sopper et al. [8]. A rough calculation based on weighting several samples and deducting a representative value for the ice holder weight yielded an average sample density of about 928 kg/m$^3$.

### Environmental Testing Conditions

#### Surrounding Water

Submerged tests were done in salt water. It was preferred to fresh water based on its lower freezing point that allowed colder testing temperatures. This mitigated the risk of inducing thermal stresses originating from large temperature gradients between ice and water. Furthermore it facilitated a longer testing window. The water temperature was manually regulated by replacing parts to prevent it from freezing.

Water salinity and temperature were measured before each sample was positioned, using a Traceable® Salinity Meter by Fisher Science Education. Salinities ranged between 20.6 ppt and 37.6 ppt at temperatures between -1.6°C and 3.6°C.

At the time of first contact between ice specimen tip and indenter, 20° cones were entirely submerged, and 30° ice cones to about 83 %.

#### Snow and Granular Ice (Chips)

The snow material was obtained from the processing of the raw ice samples. During shaping, the redundant material was expelled in form of dry snow with grains of 1 mm and less in size. Granular ice or ice chips, respectively, consisted of the same material that was used for seeding the ice specimens. Generic ice cubes were reduced to smaller chips using an ice crushing machine. The grains sizes ranged from snow with less than 1 mm up to above 10 mm. The grain size distribution was not further determined.

Both types of materials were loosely filled into the container up to a layer thickness of approx. 2 cm. After each snow test, large ice pieces were removed and a new layer created. For granular ice tests the entire material was exchanged after every run.

## Data Acquisition

### *MTS Machine*

The load cell located in the crosshead of the MTS machine was a 661 Series High Capacity Force Transducer, measuring vertical force. It had a capacity of recording tension and compression forces up to 5000 kN.

The piston of the MTS machine was a Series 244.41 Hydraulic Actuator, rated for up to 500 kN force. The vertical movement was registered by an internal linear variable displacement transducer (LVDT).

Time, force and displacement data were transmitted to a stationary computer located outside of the cold room. Low speed tests (1 mm/s) were sampled at 2048 Hz, medium (10 mm/s) and high indentation rate tests (100 mm/s) at 4096 Hz.

### *Tactile Pressure Sensors*

Tactile pressure sensors (Tekscan I-Scan® sensors model 5101) were incorporated in 26 tests and facilitated the gathering of qualitative information on local pressure patterns and contact areas during the impacts.

The sensors were rated for pressures up to 5000 psi (34.47 MPa) with a physical turn on threshold of approx. 60 psi (0.41 MPa). The matrix area for a single sensor was 111.8 mm x 111.8 mm with a total number of 1936 sensels. In each test, two facing sensors were employed to cover a larger area. Yet, it was insufficient to capture the entire contact area at advanced displacements. The sensor tabs were guided through small slots previously cut into the acrylic windows of the aluminum container and that were subsequently sealed with silicone. Outside of the container the tabs were inserted into the USB handles (Figure 1) that transmitted the information to a laptop outside of the cold room. The maximum sampling frequency was limited to 100 Hz by the equipment. Special software (Tekscan I-scan Version 7.5, Serial # 33954) was used for processing the sensor outputs. Map 5101D allowed the interconnection of the two individual sensors to one large sensing area with only a small gap in the interface where no information was acquired.

For protection from shear forces, puncture and water, the sensors were covered with a thin layer (0.05 mm) of clear moisture-resistant polyester (Mylar) which is identical to the sensor material. Its adhesive back served to fix the sensors on the indenter surface.

### *High Speed Camera (HSC) and Still Photos*

Black and white high speed camera (HSC) footage was obtained from a camera located inside the cold room. Halogen lamps, attached to the container ensured proper lighting. HSC recordings from tests with snow and granular ice were unusable since the impact was entirely concealed by the additional material.

Still photos were taken before and after each test to monitor specimen constitution and examine the contact area after the crushing.

## TEST PROCEDURE

Table 1 is a summary of all 71 performed tests. D and S indicate dry and submerged tests. Impact speeds were 1 mm/s, 10 mm/s and 100 mm/s. Low and high indentation rates were employed in all four testing environments. The medium indentation rate was mainly used in dry and submerged contact conditions, but only in single runs with granular ice for both ice cone angles.

The maximum penetration depth for 20° cones was 40 mm, for 30° cones 65 mm. Nevertheless, in tests with snow and granular ice the realized penetration was often less due to inaccuracies in determining the exact material layer thickness. Less penetration was accepted to avoid the risk of a collision between the ice holder and the indenter.

### Dry, Snow and Granular Ice (Chips) Tests

In dry, snow and chips tests the ice specimen was positioned with the tip just above the indenter or the material surface (Figure 2). The anticipated indentation rate as well as data acquisition were triggered from the very beginning until the maximum displacement was reached.

### Submerged Tests

In submerged tests, the water level was measured first. Then the specimen was positioned in a way that its tip was just not touching the water (Figure 2 top right). This value determined the distance that the sample had to travel through the water before first impact would occur. In that part, all ice specimens were moved at a constant rate of 10 mm/s to ensure that the duration of the exposure to the water was similar among tests. Approx. 5 mm before first ice-indenter contact was expected the rate was switched to the anticipated test velocity (or maintained constant). This was to account for measurement and positioning inaccuracies, to allow some reaction time for the MTS machine, and it defined the point when the data acquisition system was triggered.

**Table 1:** Overview of 71 performed tests and test parameter.

| Test Number Ov. | Day | Cone [°] | Ind. Rate [mm/s] | Ice Strength [MPa] | Cond. | Water Sal. [ppt] | Temp. [°C] |
|---|---|---|---|---|---|---|---|
| 6 | 1 | 30 | 1 | 7.4 | D | - | - |
| 7 | 2 | 30 | 100 | 2.8 | D | - | - |
| 8 | 3 | 30 | 1 | 7.6 | D | - | - |
| 9* | 4 | 30 | 100 | - | D | - | - |
| 10 | 1 | 20 | 1 | 7.8 | D | - | - |
| 11 | 2 | 20 | 100 | 1.9 | D | - | - |
| 12 | 3 | 20 | 1 | 8.9 | D | - | - |
| 13 | 4 | 20 | 100 | 3.4 | D | - | - |
| 14 | 5 | 20 | 10 | 4.0 | D | - | - |
| 15 | 1 | 30 | 1 | 9.5 | S | 30.3 | +1.6 |
| 16 | 2 | 30 | 100 | 5.1 | S | 30.4 | -1.1 |
| 17 | 1 | 20 | 1 | 13.7 | S | 28.9 | +1.6 |
| 18 | 2 | 20 | 100 | 7.0 | S | 29.0 | -0.9 |
| 19 | 3 | 30 | 1 | 7.4 | S | 31.8 | +3.4 |
| 20 | 4 | 30 | 100 | 3.5 | S | 30.9 | +0.1 |
| 21 | 1 | 20 | 100 | 3.1 | D | - | - |
| 22 | 2 | 30 | 100 | 2.8 | D | - | - |
| 24 | 2 | 30 | 100 | 2.0 | D | - | - |
| 25 | 3 | 20 | 1 | 10.7 | D | - | - |
| 26 | 4 | 20 | 100 | 3.5 | D | - | - |
| 27 | 5 | 30 | 100 | 4.6 | S | 26.8 | +1.8 |
| 28 | 6 | 30 | 1 | 7.5 | S | 26.6 | -1.2 |
| 29 | 1 | 20 | 10 | 6.1 | D | - | - |
| 30 | 2 | 20 | 10 | 5.2 | D | - | - |
| 31 | 3 | 30 | 100 | 5.9 | S | 35.3 | +1.9 |
| 32 | 4 | 30 | 1 | 7.1 | S | 36.8 | -1.2 |
| 33 | 5 | 20 | 1 | 10.2 | S | 37.6 | +1.3 |
| 34 | 6 | 20 | 100 | 5.3 | S | 36.9 | -0.6 |
| 35 | 1 | 20 | 1 | 10.9 | D | - | - |
| 36 | 2 | 30 | 100 | 2.3 | D | - | - |
| 37 | 3 | 20 | 100 | 3.5 | D | - | - |
| 38 | 4 | 30 | 1 | 7.0 | D | - | - |
| 39 | 1 | 30 | 1 | 9.0 | S | 31.0 | +1.2 |
| 40 | 2 | 20 | 1 | 13.5 | S | 32.4 | -1.6 |
| 41 | 3 | 20 | 100 | 8.0 | S | 32.8 | +3.6 |
| 42 | 4 | 30 | 100 | 6.8 | S | 31.9 | +0.1 |
| 73[P] | 1 | 30 | 1 | 7.7 | D | - | - |
| 74[P] | 2 | 20 | 10 | 3.3 | D | - | - |
| 75[P] | 3 | 30 | 10 | 4.2 | D | - | - |
| 76[P] | 4 | 20 | 100 | 2.3 | D | - | - |
| 77[P] | 5 | 30 | 100 | 3.0 | D | - | - |
| 78[P] | 6 | 20 | 1 | 8.0 | D | - | - |
| 79[P] | 7 | 30 | 10 | 2.9 | D | - | - |
| 80[P] | 8 | 30 | 1 | 9.5 | Snow | - | - |
| 81[P] | 9 | 30 | 100 | 2.9 | Snow | - | - |
| 82[P] | 1 | 20 | 100 | 8.3 | Snow | - | - |
| 83[P] | 2 | 20 | 1 | 15.6 | Snow | - | - |
| 84[P] | 3 | 30 | 100 | 3.3 | Snow | - | - |
| 85[P] | 4 | 20 | 100 | 5.3 | Snow | - | - |
| 86[P] | 5 | 30 | 1 | 11.1 | Snow | - | - |
| 87[P] | 6 | 20 | 1 | 16.1 | Snow | - | - |
| 88 | 1 | 30 | 10 | 4.7 | S | 28.9 | -0.2 |
| 89 | 2 | 20 | 10 | 4.4 | S | 29.0 | -1.5 |
| 90 | 3 | 20 | 10 | 3.8 | S | 29.5 | -1.6 |
| 91 | 4 | 30 | 10 | 4.7 | S | 24.8 | +1.1 |
| 92[P] | 1 | 20 | 100 | 7.4 | S | 20.6 | +2.0 |
| 93[P] | 2 | 30 | 1 | 8.0 | S | 21.7 | +1.1 |
| 94[P] | 3 | 20 | 1 | 11.2 | S | 21.6 | -0.2 |
| 95[P] | 4 | 30 | 100 | 2.6 | S | 22.2 | -0.9 |
| 96[P] | 5 | 20 | 10 | 7.1 | S | 21.4 | +1.1 |
| 97[P] | 6 | 30 | 10 | 4.8 | S | 21.3 | ±0.0 |
| 98[P] | 1 | 30 | 1 | 10.9 | Chips | - | - |
| 99[P] | 2 | 20 | 1 | 17.4 | Chips | - | - |
| 100[P] | 3 | 30 | 100 | 4.0 | Chips | - | - |
| 101[P] | 4 | 20 | 100 | 9.1 | Chips | - | - |
| 102 | 5 | 30 | 100 | 4.8 | Chips | - | - |
| 103 | 6 | 20 | 1 | 13.5 | Chips | - | - |
| 104 | 7 | 20 | 100 | 5.5 | Chips | - | - |
| 105 | 8 | 30 | 1 | 10.8 | Chips | - | - |
| 106 | 9 | 20 | 10 | 6.1 | Chips | - | - |
| 107 | 10 | 30 | 10 | 4.1 | Chips | - | - |

\*    Test excluded from the analysis.
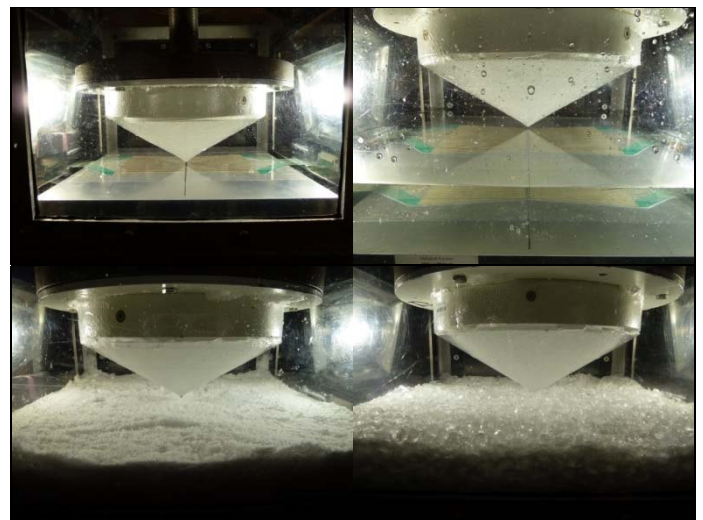P    Tactile pressure sensor measurements available.



**Figure 2:** Still photos of positioned specimens for dry (top left), submerged (top right), snow (bottom left) and granular ice (bottom right) contact conditions for 30° ice cone angle.

## DATA ANALYSIS

The data was analyzed using a dedicated code that was written in Matlab® R2014b. The code was developed for processing time, displacement and force data as it was obtained from the MTS machine (*.dat files). Among other parameters, main user input comprised the determination of first impact by means of the raw force-time history for each test. That instant was identified as the point when the force started to deflect. Forces before that point were averaged and served as a tare value to normalize the subsequent force history. Time and displacement were also normalized to this point.

The analysis code included a spectral analysis of the force histories with a Fast Fourier Transform (FFT). None of the tests revealed a dominant frequency but several high speed tests indicated some distortions in higher frequency ranges. For that reason a low pass filter at 200 Hz was applied to all data.

For the analysis, displacements were limited to 35 mm and 60 mm for 20° and 30° ice specimens to account for cone tip imprecisions and measurement tolerances. However, data from tests with snow and granular ice do often not cover the entire range for the previously explained reasons.

One case, as indicated in Table 1, test D T09-04 was excluded from the analysis. This test produced suspiciously low forces between 8.5 mm and 20.6 mm displacement and was regarded as an outlier.

In a separate code the average ice strength dependent on indentation rate for each external boundary condition was calculated. In a first step, the force was integrated to derive the crushing energy. Next, based on the displacement a nominal ice volume was calculated. By setting the energy in relation to the volume, the nominal ice crushing strength was obtained.

## RESULTS

Figures 3 through 8 show force-displacement histories for 20° (left) and 30° (right) ice specimen angles. The y-axis goes up to 400 kN force. The figures display from the top to the bottom the three indentation rates in ascending order. Dry and submerged tests are shown in green and blue shaded areas. The number of tests represented by the shaded areas is indicated by the numbers in brackets in each figure caption. The single tests with snow and granular ice (chips) are individually provided (snow: dots, chips: dashed).

Figure 3 is based on 13 tests that were performed with 20° ice specimens at 1 mm/s indentation rate. Despite some overlap, loads in submergence (blue) are higher than those for a dry contact condition (green). Yet, it is evident that snow or granular ice (chips) produced even higher forces. Snow test T83-02 has three distinct drops but loads quickly return to similar magnitudes before these events happened. Only chips test T103-06 is low compared to other tests with snow and chips, but is of similar in magnitude to the submergence case.

Figure 6 for 30° ice specimens (15 tests) reveals the same trends. Despite some more overlap, loads in submergence cases are generally higher than for the dry contact surface, and yet, are exceeded by snow and granular ice cases. First snow is above granular ice. This ratio reverses starting from approx. 38 mm displacement until the curves prematurely terminate because of insufficient penetration depth. However, the tendency indicates that this ratio would remain.

Figure 4 (8 tests) and Figure 7 (6 tests) display 10 mm/s indentation rate. In these cases a trend of higher ice loads in submergence is only evident at 30° ice cone angle. In both cases the single granular ice test yields forces that are in the mid-range of the other two contact conditions.

Figure 5 (14 tests) for 100 mm/s indentation rate and with 20° ice specimens most evidently displays increased ice loads in submergence cases, compared to a dry contact surface. The difference intensifies with advancing displacement. Also snow and granular ice show high forces but they are comparable to the submerged condition. Snow test T85-04 is low and closer to dry tests up to 28 mm displacement. It then converges to the other snow test, with similar loads to the submergence case, as the test proceeds.

A comparable trend can be seen in Figure 8 (16 tests) for 30° specimens. Submerged loads are consistently higher than dry loads, but in contrast to 20° cones, there is more overlap at advanced displacement. In that case loads from the snow and granular ice cases are closer to the dry condition. This is true for granular ice up to 36 mm penetration when forces rise and approach those in the submergence cases.

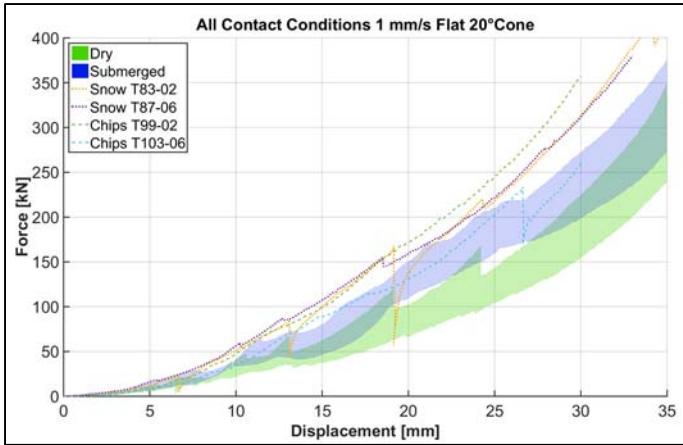## FORCE VS. DISPLACEMENT
**20° Ice Specimens**

**Indentation Rate: 1 mm/s**



**Figure 3:** 1 mm/s, 20° cone: dry (5), submerged (4).
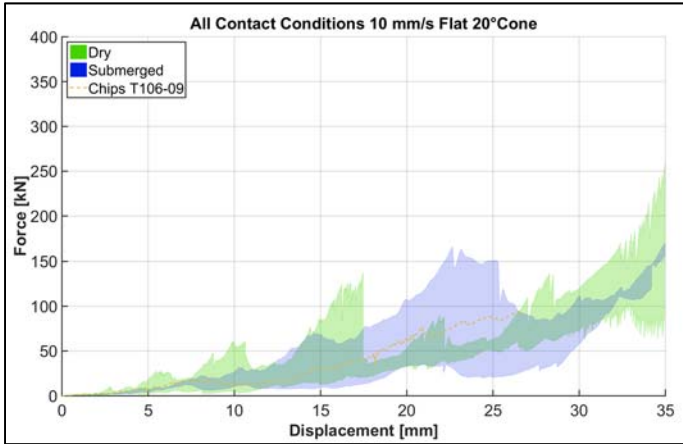
**Indentation Rate: 10 mm/s**



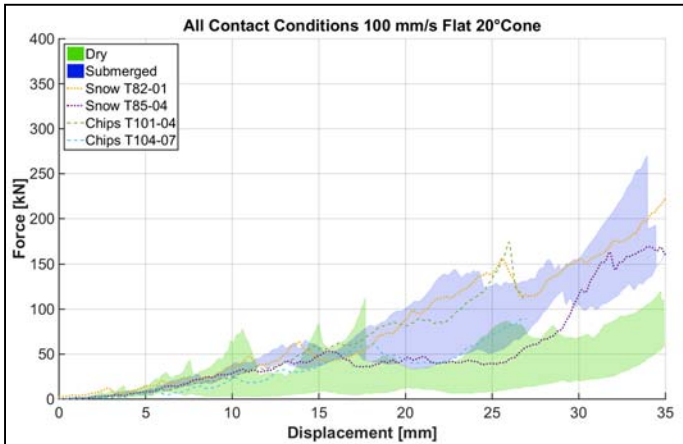**Figure 4:** 10 mm/s, 20° cone: dry (4), submerged (3).

**Indentation Rate: 100 mm/s**



**Figure 5:** 100 mm/s, 20° cone: dry (6), submerged (4).
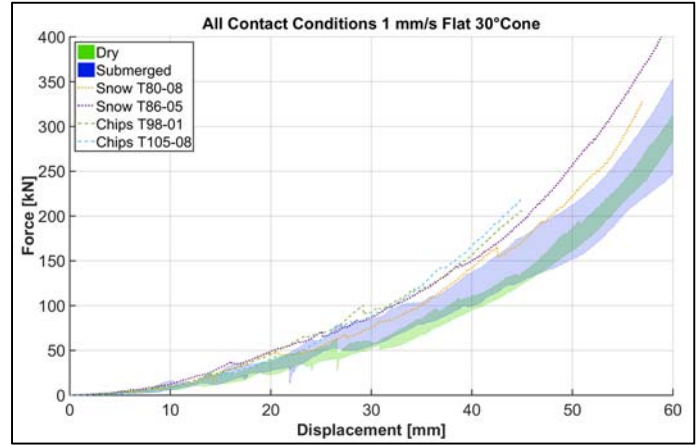
**30° Ice Specimens**

**Indentation Rate: 1 mm/s**



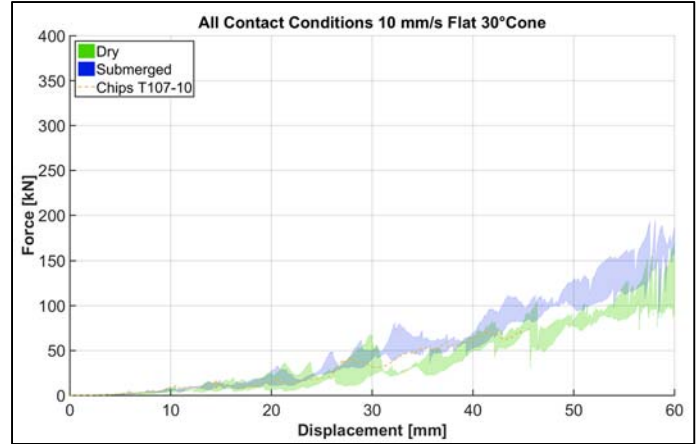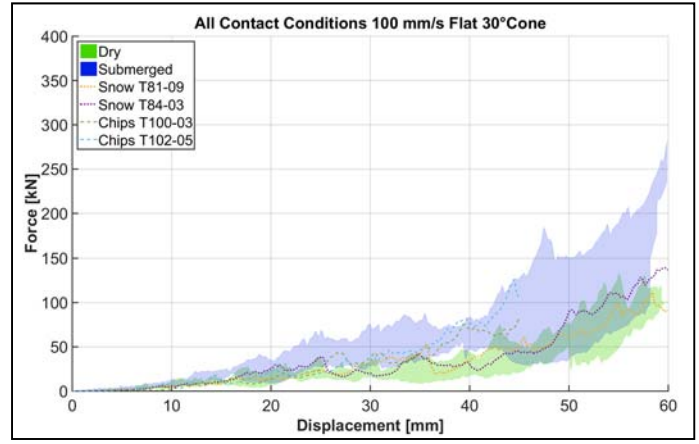**Figure 6:** 1 mm/s, 30° cone: dry (4), submerged (6).

**Indentation Rate: 10 mm/s**



**Figure 7:** 10 mm/s, 30° cone: dry (2), submerged (3).

**Indentation Rate: 100 mm/s**



**Figure 8:** 100 mm/s, 30° cone: dry (5), submerged (6).

## DISCUSSION

The above results reveal a distinct trend: ice loads in dry ice-structure interactions are consistently lower compared to those where water, snow or granular ice are present as external boundary conditions. Submergence causes higher ice loads in general, but especially at the high indentation rate (100 mm/s). Also snow and granular ice on the indented surface yield increased loads which are more pronounced at the low indentation rate (1 mm/s). Obviously, the importance of the respective contact condition depends on impact velocity. The following explanations focus on high and low indentation rates where the most significant differences were noticed.

### Indentation Rate

Generally, the low indentation rate causes higher loads. Examples are provided with Figure 9 and Figure 10 that display force vs. displacement for the three employed impact velocities (green: 1 mm/s; blue: 10 mm/s; red: 100 mm/s) for 20° ice specimens but for different contact conditions. For a dry contact surface (Figure 9) loads diminish with increasing rate. This order does not apply to a submerged environment as it is evident in Figure 10. Forces at 100 mm/s are now higher than at 10 mm/s and clearly shifted towards those at 1 mm/s. On the other hand, loads at 1 mm/s are only slightly elevated in submergence and reach roughly 275 – 375 kN at the final displacement in both testing environments. A similar trend but not as pronounced is true for 30° ice specimens (no figures provided).

### Contact Area and Local Pressure Patterns

In these tests, the ice load magnitude in all cases correlates with the size of contact area. Increased loads always correspond with a simultaneous gain in contact area, independent of contact condition or indentation rate.

Low impact velocities result in ductile ice failure. At the immediate ice-structure interface, ice recrystallization and ice sintering take place and facilitate the development of a large contact area. These processes may explain the dramatically increased ice loads at the low indentation rate in the presence of snow or granular ice on the indenter surface. During the creeping and recrystallization of the ice, snow and granular ice provide additional material sources that are incorporated into the ice specimen. Still photos of samples after the tests indicate enlarged contact areas compared to the dry case. Figure 11 shows four samples after testing with lighting applied from the back. The circular shape of the contact area is characteristic for conical ice impact test at low rates and is consistent for all testing environments. The difference is, though, that contact areas in the bottom two images (snow and granular ice) are distinctly larger compared to the ones in the top photos (dry and submerged) although in these cases less penetration stroke was achieved.
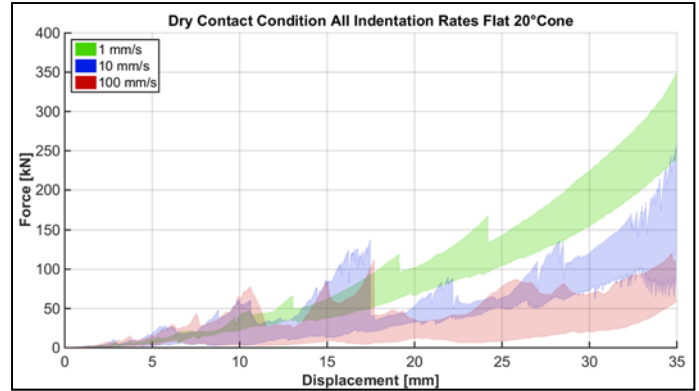


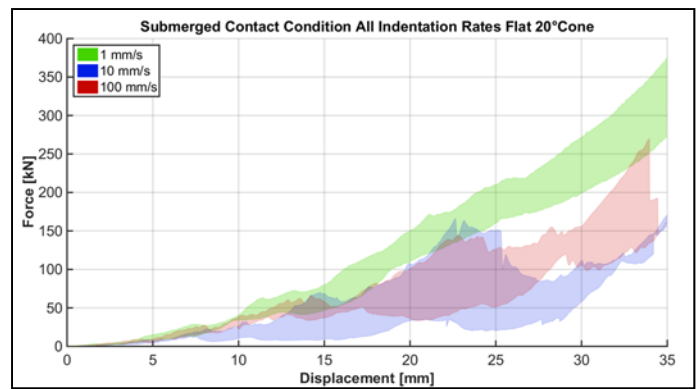**Figure 9:** 20° specimens: 1 mm/s (5), 10 mm/s (4) and 100 mm/s (6).



**Figure 10:** 20° specimens: 1 mm/s (4), 10 mm/s (3) and 100 mm/s (4).
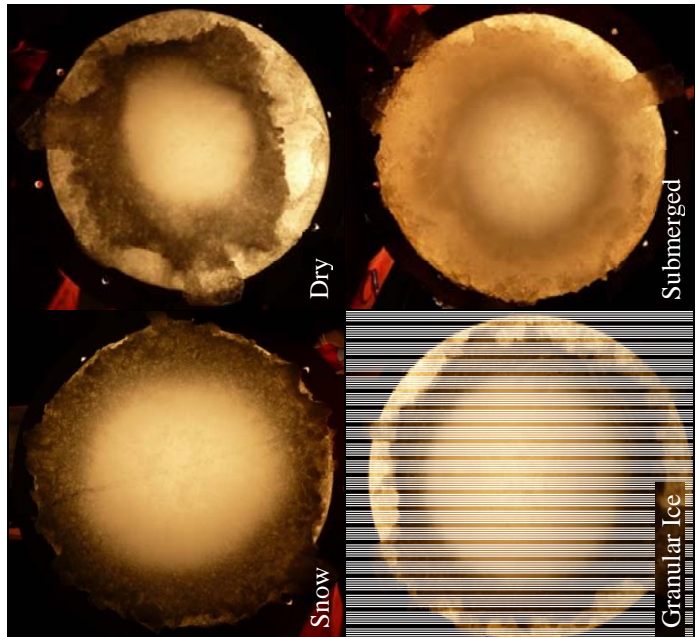


**Figure 11:** 1 mm/s, 20° ice specimens: images of samples after testing with lighting applied from the back. (D T78_06, S T94_03, Snow T83_02, Chips T99_02).

The increased contact area is also clearly evident in the measurements from the tactile pressure sensors. Figure 13 displays examples for each testing environment and for 30° ice specimens. It is mentioned that due to equipment failure only one pressure sensor measurement is available for tests with granular ice. Furthermore, in submerged tests one sensel column broke causing its saturation which is visible by means of a red vertical line. Measurements up to that margin are unbiased, but contact areas reaching or crossing that border have to be discarded. Also note that all pressure patterns presented in this paper are scaled to a raw pressure of 110 (Figure 12) and processed with a 5 x5 interpolation.

The snap shots in Figure 13 are derived at a penetration depth of roughly 38 mm as it is the last evaluable frame for the submerged test. Dry and submerged (top) are comparable in terms of contact area size. This correlates with the very similar force measurements in Figure 6. Snow test T80-08 (bottom left) seems slightly larger and to be somewhat extended in the lower right half. Yet, at approx. 38 mm displacement Figure 6 shows a faintly higher load than in the previous two cases. At the same displacement, the contact area of granular ice test T98-01 is visibly larger than all others and exceeds the sensing area on top and bottom. Concurrently higher forces are obtained (Figure 6) for this test.
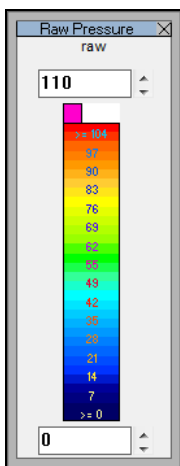


Differences are also apparent regarding the local pressures distributions that will be qualitatively discussed. In the dry testing environment (top left) there is one large high pressure zone (HPZ) in the center (red color) with outwards declining pressures. That pattern is similar for submergence and snow, although the HPZs seem to be somewhat mitigated. Granular ice, on the other hand, does not follow that trend. Here, pressures are locally lower and one center HPZ is non-existent. Despite the lower pressures, loads measured for this test are high.

**Figure 12:** Raw scale of pressure measurements.

High impact velocities are generally described to cause brittle ice failure that is characterized by sudden ice spall events and ice extrusion. The tests of this study imply that this does not equally apply to high rate impacts in submergence cases.

Figure 14 contains screen shots of HSC recordings of 20° ice specimens crushed in dry and submerged conditions at 100 mm/s. In the dry environment (top) clearly visible is the extrusion of fine grained ice, spread out over the entire indenter surface.
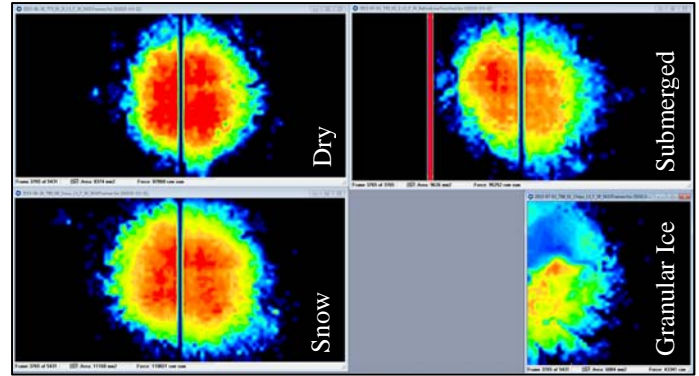


**Figure 13:** 1 mm/s, 30° ice specimens: pressure patterns in approx. 37.65 mm penetration depth for all contact conditions. (Top) left: dry T73-01, right: submerged T93-02; (Bottom) left: snow T80-08, right: granular ice T98-01.

The picture is very different in submergence (bottom). Thereby the water appears to have two main effects: firstly, it alters the ice debris constitution. Instead of distinguishable and widely spread ice grains, the ice debris seems cloud-like and remains in close vicinity to the contact area. Secondly, the viewings of HSC videos indicate the impediment of crack development and propagation. Cracks occur mostly near the ice-indenter interface and seldom penetrate the entire ice specimen. If a large ice spall is formed the water prevents its separation from the ice specimen body, likely due to the combination of two effects. One is a back pressure that is applied by the water and that simply keeps the spall in place; that is to say the water confines the expulsion of ice spalls. The other is that the evolving crack between the ice spall and the parent specimen is very small and is quickly penetrated by water. The thermal capacity of the ice is probably sufficient to cause refreezing, thus establishing a new bond between both ice features.

At the outset of the study, the different degree of submergence (100 % for 20°, about 83 % for 30° ice specimens) at the time of first impact was not expected to be of concern. The noticed change in crack development and propagation may imply otherwise. However, it is believed that the extent to which this circumstance may have affected the results is considerably mitigated due to the observed restriction of cracks closer to the ice-indenter interface. It is also mentioned that for none of the tests a relation to water temperature was found.
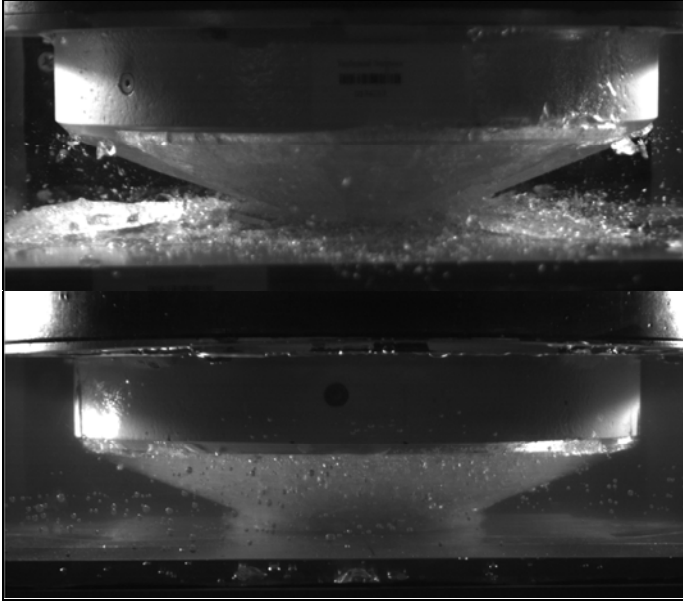
**Figure 14:** 100 mm/s, 20° ice specimens, HSC footage: dry (top, D T76-04) and submerged (bottom, S T92-01), approx. 14.4 mm penetration depth. The photos contrast the altered ice debris development and extrusion in submergence compared to the dry condition.

Pressure patterns at high indentation rate are commonly described to have a branch-like shape with quickly shifting HPZs. Those are due to the sudden fracture and spalling events that result in sudden contact area losses and limit the overall contact area. The test results also indicate that this is changed in submergence, as it is evident in the pressure patterns in Figure 15. The images display a dry (top) and a submerged test (bottom), with the left and right pictures at approximate indentation depths of 7 mm and 23 mm. From the photos on left it can be seen that while the contact area of the dry test is small and is U- or V- shaped, the one of the submerged test is larger and more compact.

The size difference intensifies with proceeding penetration as it is displayed in the images on the right. The dry test exhibits the characteristic branch-like pattern with (small) HPZs that are enclosed in zones of lower pressures (LPZs). Viewing the recordings shows that those HPZs quickly shift due to sudden ice spalling events. The blue dots in the surroundings originate from extruded ice spalls and ice debris as it is visible in the HSC footage (Figure 14, top). In contrast, the contact area of the submerged test is many times larger and essentially round. The overall characteristic is basically the same as the pattern from the low indentation rate: circular and very compact (compare Figure 13). The internal local pressure pattern, does display a distinct line-like HPZ, with signs of branching out. At other times during the impact, as well as in other tests in general, the HPZs are not necessarily that continuous or line-like. Still, overall in submergence HPZs

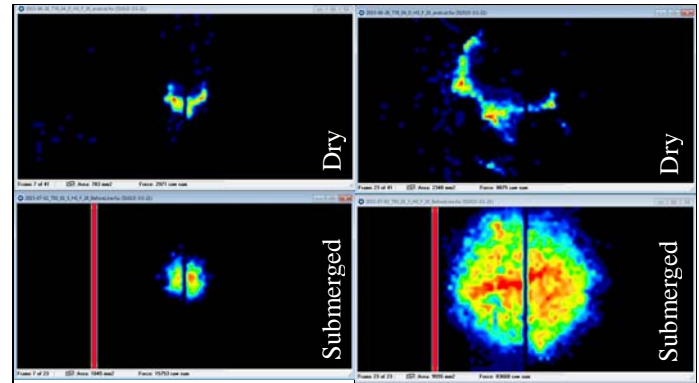often appear to be more pronounced and numerous within the larger pressure area.



**Figure 15:** 100 mm/s, 20° ice specimens: pressure patterns in approx. 7 mm (left) and 23 mm (right) penetration depths. (Top) Dry test D T76-04, (Bottom) submerged test S T92-01. The images show the distinctly increased contact area in submergence, especially at more advanced penetration.

**Ice Strength**

The ice crushing strength of every individual test is determined by integrating the force over the entire test length divided by the nominal crushed ice volume. The individual values in Table 1 are summarized to an average ice crushing strength for each external boundary condition. Figure 16 and Figure 17 present the results separately for 20° and 30° ice specimens with error bars indicating the respective standard deviation (where available). The markers are slightly misaligned over the related indentation rate to provide a better overview.

Overall, 20° ice cones are stronger than 30° ice cones, but both graphs reveal that the ice is generally the weakest for a dry boundary condition (green). In submergence cases (blue), the ice is stronger, especially at the high indentation rate. With snow (black) or granular ice (magenta) at the ice-indenter interface, the ice is considerably stronger at the low indentation rate. At the high indentation rate, on the other hand, those environments cause ice strengths comparable to those observed for submergence cases. This is most pronounced for 20° ice specimens. In that case, there is also more variance among the tests with snow and granular ice, compared to dry or submerged cases. For 30° ice specimens at the high indentation rate, snow and a dry surface lead to lower average ice strengths, while submergence and granular ice yield somewhat higher values.

It is interesting that for a dry boundary condition, the ice strength continuously declines with increasing impact velocity, while in submergence cases, or with granular ice, the ice strength decreases from 1 mm/s to 10 mm/s, but rises or remains roughly constant with increasing velocity. The comparable trend for snow is unknown since no information at the medium indentation rate was obtained.
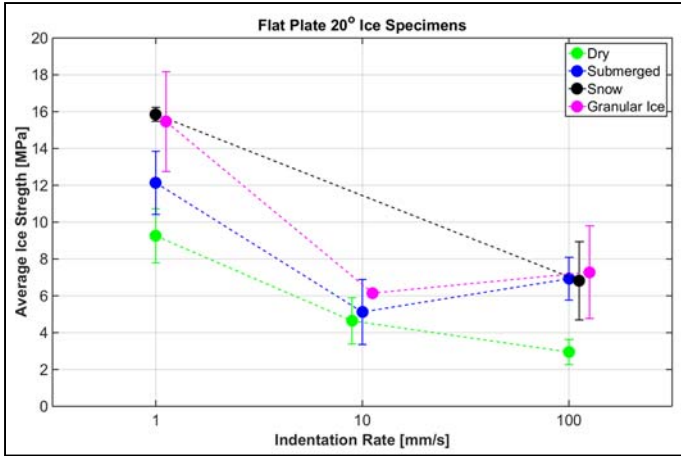
**Figure 16:** 20° ice specimens: average ice strength vs. indentation rate for all external boundary conditions**.**
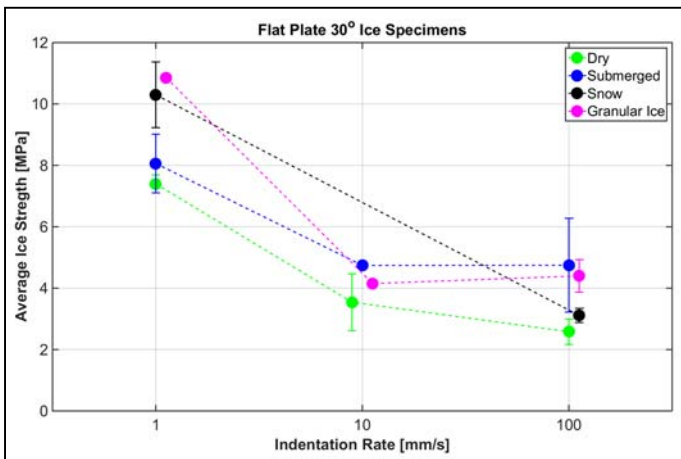


**Figure 17:** 30° ice specimens: average ice strength vs. indentation rate for all external boundary conditions.

## CONCLUSIONS AND RECOMMENDATIONS

The objective of this study was to assess the influence of different external boundary conditions on ice load magnitude. In total, 71 laboratory tests were performed: 27 dry, 26 submerged, and 8 and 10 with respectively snow and granular ice on the indenter surface. Impact speed was varied with 1 mm/s, 10 mm/s, and 100 mm/s.

Independent of indentation rate, the lowest ice loads were always obtained for a dry ice-indenter interface. Those were generally exceeded by impacts in submergence cases. This was especially pronounced at high indentation rates. Furthermore, high loads were obtained with snow and granular ice on the indenter surface, most noticeable at the low indentation rate. In all cases, an increased force correlated with a larger contact area. This was attributed to different physical mechanisms dependent on testing environment.

In submergence, the water influenced the constitution of ice debris, restricted the clearance of ice spalls, and impeded

crack development and propagation within the ice specimen. Furthermore, the water seemed to support the occurrence of HPZs which were larger and more numerous.

Snow or granular ice on the indenter surface appeared to provide an additional load bearing material source. Presumably recrystallization and sintering processes lead to the incorporation of the surrounding ice materials into the ice specimen body thus enlarging the contact area and allowing more load transmission.

The results offer evidence that external boundary conditions are a significant factor with respect to ice load magnitude but also in view of internal pressure patterns. More research is needed to further elucidate the observed phenomena and to establish relationships that would allow the quantification of these effects in ice load determinations.

In future experiments more attention should be paid to the water level. As submergence appeared to affect crack development and propagation, the degree to that the ice specimens are submerged at the time of first contact may be of some influence.

This study only worked with dry snow and granular ice material that was loosely filled into the aluminum container. For a better representation of natural circumstances it would be an improvement to experiment with wetted or consolidated material.

Future tests could also involve higher speed ranges as well as larger scales. In all cases it is desirable to involve pressure sensing technologies that offer information on local pressure patterns and contact area, as these seem to be the essential factors that are influenced by the boundary conditions and thus control the applied load.

## REFERENCES

[1] Hill, B. T. 2006. *Ship collision with iceberg database*. International Conference and Exhibition on Performance of Ships and Structures in Ice (ICETECH 2006), Anchorage, Alaska, USA.

[2] Masterson, D. M., and R. M. W. Frederking. 1993. *Local contact pressures in ship/ice and structure/ice interactions*. Cold Regions Science and Technology 21 (2) (1): 169-85.

[3] Ritch, R., R. Frederking, F. Johnston, F. Browne, and F. Ralph. 2008. *Local ice pressures measured on a strain gauge panel during the CCGS terry fox bergy bit impact study*. Cold Regions Science and Technology 52 (1): 29-49.

[4] Frederking, R., I. J. Jordaan, and J. S. McCallum. 1990. *Field tests of ice indentation at medium scale Hobsons's Choice ice island, 1989*. Proceedings International Association for Hydraulic Research, IAHR '90, Espoo, Finland.

[5] Masterson, D. M., R. M. W. Frederking, I. J. Jordaan, and P. A. Spencer. 1993. *Description of multi-year ice indentation tests at Hobsons's choice ice island - 1990*. Proceedings of the 12th International Conference on Offshore Mechanics and Arctic Engineering, Glasgow, Scotland.

[6] Kennedy, K. P., I. J. Jordaan, M. A. Maes, and A. Prodanovic. 1994. *Dynamic activity in medium-scale ice indentation tests*. Cold Regions Science and Technology 22 (3): 253-67.

[7] Varsta, P. 1983. *On the Mechanics of Ice Load on Ships in Level Ice in the Baltic Sea,* Espoo, Technical Research Centre of Finland.

[8] Sopper, R., C. Daley, and B. Colbourne. 2015. *Ice loads in dry and submerged conditions*. Proceedings of the 34th International Conference on Ocean, Offshore and Arctic Engineering (OMAE), St. John's, Newfoundland, Canada.

[9] Tuhkuri, J., and K. Riska. 1990. *Results from tests on ice extrusion of crushed ice*. Otaniemi: Helsinki University of Technology, Faculty of Mechanical Engineering, Laboratory of Naval Architecture and Marine Engineering, M-98.

[10] Spencer, P. A., D. M. Masterson, J. Lucas, and I. J. Jordaan. 1992. *The flow properties of crushed ice: Experimental observation and apparatus*. Proceedings International Association for Hydraulic Research, IAHR '92, Banff, Alberta, Canada.

[11] Singh, S. K., and I. J. Jordaan. 1996. *Triaxial tests on crushed ice*. Cold Regions Science and Technology 24 (2): 153-65.

[12] Daley, C., J. Tuhkuri, and K. Riska. 1996. *Discrete chaotic ice failure model incorporating extrusion effects*. National Energy Board.

[13] Bruneau, S. E., Dillenburg, A.K., Ritter, S. 2012. *Ice sample production techniques and indentation tests for laboratory experiments simulating ship collisions with ice.* International Offshore and Polar Engineering Conference, 17-22 June 2012, Rhodes, Greece.